Journal of Fluids and Structures (1998) **12,** 537–547
Article No. fl980159

ANALYSIS OF ATMOSPHERIC WIND AND PRESSURES ON A LOW-RISE BUILDING

M. R. Hajj

Department of Engineering Science and Mechanics, Virginia Tech Blacksburg, VA 24061–0219, U.S.A.

D. A. Jordan

School of Engineering and Applied Science, University of Virginia Charlottesville, VA 22903, U.S.A

H. W. Tieleman

Department of Engineering Science and Mechanics, Virginia Tech Blacksburg, VA 24061–0219, U.S.A

(Received 20 June 1997 and in revised form 6 April 1998)

Modelling the relation between turbulence scales in atmospheric wind and surface pressures on low-rise buildings is important for prediction of wind loads on structures. Because the interest is in events that take place over short time periods, wavelet analysis is performed to characterize this relation. The Morlet wavelet transform is applied to simultaneously measured velocity components of atmospheric wind and surface pressures at multiple locations on a low-rise building. The wavelet energy density of the individual time series show that both atmospheric turbulence and pressure fluctuations are highly intermittent, i.e. the energy of the different scales in these fluctuations varies significantly with time. Furthermore, the low-pressure peaks are represented by high levels of the wavelet energy density. Cross-scalogram results show that there is a clear relationship between energetic events in the atmospheric wind and low-pressure peaks that occur simultaneously at pressure taps placed over a large area of the low-rise building. Specifically, there is a scale relation between the u- and v-velocity components of the incident wind and the pressure fluctuations. Such results show that better prediction of pressure peaks can be obtained by simulating turbulence events rather than merely matching integral length scales, mean flow parameters or turbulence intensity.

1. INTRODUCTION

Experimental and numerical simulation of wind loads on the roofs of low-rise structures can be significantly enhanced by better knowledge of the relation between turbulence scales in the atmospheric surface layer and surface pressure fluctuations. In particular, it is of interest to be able to predict the occurrence of low-pressure peaks based on the characteristics of the incident flow. The nature of the pressure–velocity relation is such that one could expect to develop a relation between the far-field turbulence and the surface pressure fluctuations. Clearly, near-field flow characteristics, such as vortex formation and flow separation around the building play a major role in determining surface pressures. However, the near-field flow is also affected by the incident flow characteristics. Thus, it is

0889–9746/98/050537 + 11 $30.00

reasonable to pursue a relation between the far-field velocity characteristics and the surface pressure. Several approaches have been proposed to quantify such a relation. Strip theory gives the wind pressure as directly related to the wind velocity at the same height (Kawai 1983). Linearized quasi-steady theory gives the surface pressure fluctuations as directly proportional to instantaneous velocity and flow direction (Kawai 1983), whereas the modified (nonlinear version of) quasi-steady theory assumes that the flow is directly proportional to the squares of the instantaneous velocity components.

The complexity of the time series of the wind velocity components and the associated pressure fluctuations has led to the application of frequency domain analysis to examine these theories. However, such analysis has shown that all of the above theories fail to predict characteristics of surface pressure fluctuations in regions of flow separation and vortex formation. This, in turn, led to the introduction of empirical admittance functions to resolve the discrepancies between the theoretical predictions and experimental results. One problem with empirical admittance functions is that they are dependent on the specific experimental parameters such as geometry, Reynolds number, turbulence scales, etc. Furthermore, in our previous work, Hajj & Tieleman (1996) and Hajj *et al.* (1996), we explained the shortcomings of frequency-domain analysis in the prediction of wind loads on low-rise structures. Briefly, in the Fourier analysis, time-localized events in the pressure–velocity relation are mapped over many infinite sinusoids. Moreover, in full-scale studies, it is well known that pressure peaks take place over a time period of a few seconds which is much smaller than the time period required to obtain meaningful averaged Fourier-domain spectral moments.

In Hajj & Tieleman (1996) and Jordan *et al.* (1996) an analysis of the velocity–pressure relation based on the continuous wavelet transform was proposed, to circumvent the problems presented by frequency-domain analysis. The wavelet transform maps the signal on a time-scale plane and thus retains temporal information. The objective of this work is to use such information to answer two fundamental questions. These are: (i) *Which scales in the pressure fluctuations are associated with low-pressure peaks?* (ii) *Do these scales coincide with equivalent scales that appear at the same time in the velocity components of the incident flow?* Only the case of normal (90°) incident flow is considered here. The oblique incidence case will be considered in future work. In Section 2, brief definitions of the continuous wavelet transform and its implementation procedure in this work are presented. In Section 3, a brief description of the experimental set-up is given. The results of wavelet analysis of simultaneously measured velocity and pressure fluctuations are discussed. Conclusions drawn from this analysis are presented in Section 4.

2. DEFINITIONS AND IMPLEMENTATION PROCEDURE OF THE WAVELET TRANSFORM

Wavelets are mathematical functions that possess the properties of oscillation with zero mean and localized support (decay to zero over a finite region of the independent variable). The first property is a result of *admissibility*. The admissibility condition of a wavelet function guarantees that when a general function of time is transformed into the time-scale domain with that wavelet, then the inverse transform exists. Localized support is the property that makes wavelets useful for the analysis of time-dependent and nonstationary fluctuations. In this work, we use the Morlet wavelet, which is given by

$$\psi(t) = \exp(\mathrm{i}\omega_\psi t)\exp(-|t|^2/2), \tag{1}$$

where ω_ψ is a parameter set equal to 5·5 that gives a mean for the Morlet wavelet of $-0{\cdot}000106$ to satisfy the admissibility condition (approximately). Note that the Morlet wavelet is a complex-valued function. As illustrated with test signals by Farge (1992), the advantage of using a complex-valued wavelet over a real-valued wavelet is the elimination of oscillations of the analysing wavelet itself in the wavelet coefficients. The continuous wavelet transform of a function or signal, $f(t)$, is given by

$$\mathscr{W}(a, \tau) = \langle f(t), \psi_{a,\tau} \rangle = a^{-1/2} \int_{-\infty}^{\infty} f(t)\, \psi^* \left(\frac{t-\tau}{a} \right) \mathrm{d}t \,, \tag{2}$$

where $\psi(t)$ is the mother wavelet, a is the dilation parameter and τ is the translation parameter. The wavelet transform is a projection of $f(t)$ onto all scaled and translated versions of the single mother wavelet, $\psi(t)$. In this work the projection is done using the $\mathscr{L}^2$ norm inner product integral which results in a normalization constant of $a^{-1/2}$ in equation (2). Based on the form in equation (2), the continuous wavelet transform is computed as a set of convolution integrals, parameterized by the scale, a, which maps the original time series into a two-dimensional function in the time-scale domain. Because the experimental signals are sampled in time, the continuous wavelet transform has to be performed digitally. In the digital implementation, the integral convolution in equation (2) becomes a discrete convolution between the measured time series and sampled versions of all scaled analysing wavelets. In the implementation procedure presented by Jordan *et al.* (1997), the wavelets are sampled to preserve symmetry and are "clipped" at a cut-off, T, defined here as $3\sigma_t$, which comes from the second moment of the mother wavelet. The number of points on which the mother wavelet (defined as $a = 1$) is sampled and the sampling rate of all scaled versions of the mother wavelet ($a > 1$) is determined by aliasing considerations. An equation for the minimum number of points on which the wavelet should be sampled can be derived by requiring that the band-pass filter corresponding to the mother wavelet is less than the Nyquist frequency of the sampled time series. This number of points distributed on the wavelet from $-T$ to T determines the sampling rate of the wavelet. Since the mother wavelet has the highest frequency content, all scaled wavelets can be sampled at the same rate without aliasing. Using the procedure of populating scales outlined in Jordan *et al*, 47 values of scale, a, were spaced logarithmically in frequency. The number of time-series points used was 8192 and the largest scale was $a = 152{\cdot}9$. Because wavelet functions are represented by a band of frequencies in the Fourier domain, there is no single frequency which corresponds to scale. However, because of the band-pass filter nature of Fourier-transformed wavelets, one can determine a relationship between the scale, a, and the peak frequency, f_p, of the band-pass filter corresponding to each scaled wavelet. This relationship was derived in Jordan *et al.* (1997) and in this work, this relationship was determined to be

$$f_p = \frac{2{\cdot}90}{a} \,, \tag{3}$$

with f_p in Hz. This resulted in a peak frequency range between $1{\cdot}89 \times 10^{-2}$ and 2·90 Hz. The wavelet transform coefficients, $\mathscr{W}(a, \tau)$, represents the contribution of the scales to the signal at time τ. The wavelet energy is given by $\mathscr{W}\mathscr{W}^*$; Farge (1982) defined a wavelet energy density $\mathscr{W}\mathscr{W}^*/a$ as a measure of the energy per scale size. Its advantage is that, when integrated, it yields the global wavelet energy spectrum which gives the energy content at that scale.

For the purpose of determining the relation between velocity and pressure fluctuations, the cross-scalogram is used to obtain an indication as to the occurrence of fluctuations coinciding in scale and time for two simultaneously measured time series. From the wavelet transform coefficients, $\mathscr{W}(a, \tau)$, the cross-scalogram is defined between two functions $u(t)$ and $p(t)$ as (Hudgins *et al.* 1993)

$$\mathscr{W}(a, \tau)\,[u]\mathscr{W}^*(a, \tau)\,[p]\,, \tag{4}$$

where the asterisk denotes the complex conjugate. The interpretation of the cross-scalogram follows from a basic property of the wavelet transform. If a function is not fluctuating at a certain scale at a given time then the wavelet coefficients for that region in the time-scale domain are zero. Note that the scalogram is essentially a complex multiplication of the wavelet coefficients from the two time series:

$$\mathscr{W}(a, \tau)\,[u]\mathscr{W}^*(a, \tau)\,[p] = \rho_u e^{i\theta_u}\rho_p e^{-i\theta_p} = \rho_u\rho_p e^{i(\theta_u - \theta_p)}\,. \tag{5}$$

Therefore, the cross-scalogram magnitude is determined by the magnitudes of the individual wavelet transform magnitudes multiplied together at each point in the time-scale domain. It is clear that there must be a significant fluctuation coincident in scale and time in each time series to obtain large values of the cross-scalogram. However, one should note here that if either of the individual wavelet transforms in the cross-scalogram is nearly constant everywhere and the second is highly intermittent, then the significance of the results is reduced since the cross-scalogram will essentially reproduce the second wavelet transform. Consideration of equation (5) reveals this feature. Therefore, results are more meaningful when there is a high degree of intermittency in time and scale.

3. RESULTS AND DISCUSSION

The data presented here was taken at the Wing Engineering Research Field Laboratory (WERFL) at Texas Tech University. Simultaneously measured velocity components and pressure fluctuations at four roof taps (Figure 1) are considered. More details of the measurement setup, techniques and geometry is given in Levitan & Mehta (1991). The velocity measurements were obtained from cup-vane anemometers mounted about 4·0 m above the ground (same as roof height, H) and located 46·0 m from the centre of the experimental structure at a 180° azimuth angle. The time records of the u- and v- velocity are shown in Figure 2. Corresponding time records of the pressure coefficient at four taps are shown in Figure 3. These taps are located on the roof of the building at nondimensional distances $y/H = 0{\cdot}09$, 0·318, 0·395, and 0·545 along a line $x/H = 0{\cdot}663$ and are referred to as taps 1, 2, 3, and 4, respectively. An interesting feature of the pressure time series is the occurrence of two peaks at times near 480 and 520 s which last for a period of about 2–3 s. These peaks have a value of C_p of about $-3{\cdot}5$ for taps 1, 2 and 3 and about $-2{\cdot}5$ for tap 4. This observation is important because it shows that the pressure peaks near times 480 and 520 s take place simultaneously over a relatively large area of the roof and not just at one location. By examining the time series of Figure 2, one cannot observe distinctive events in the u- or v-components that result in these peaks. In other words, one cannot predict the appearance of pressure peaks by simply examining the velocity records. Furthermore, as shown by Hajj *et al* (1996), frequency-domain analysis could not give more information since that approach eliminates all temporal information.

The time series presented in Figures 2 and 3 were analysed using the Morlet wavelet according to the procedure presented in Section 2. Contour plots of the wavelet energy

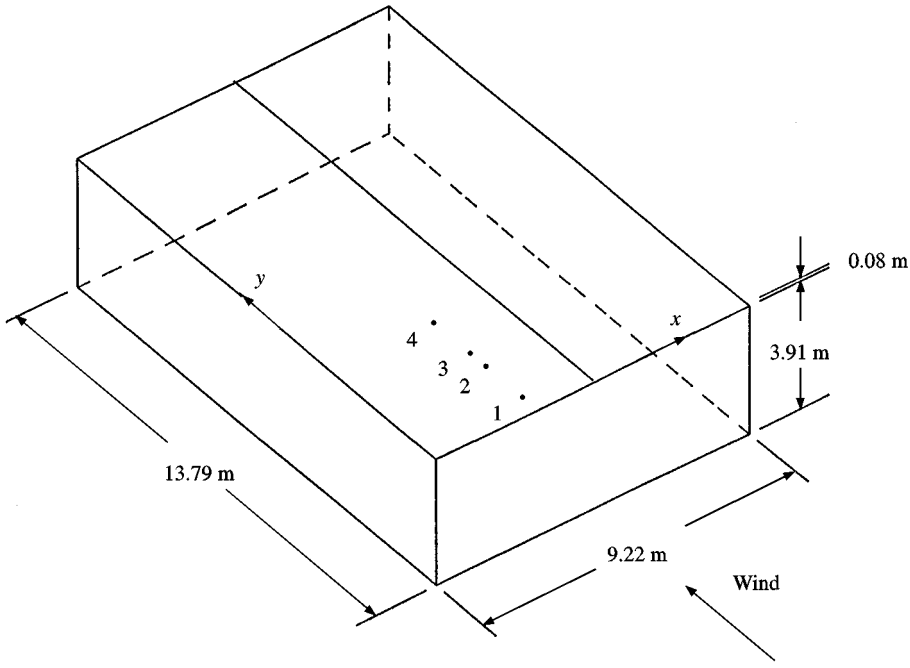

Figure 1. Texas Tech experimental building and pressure tap locations.

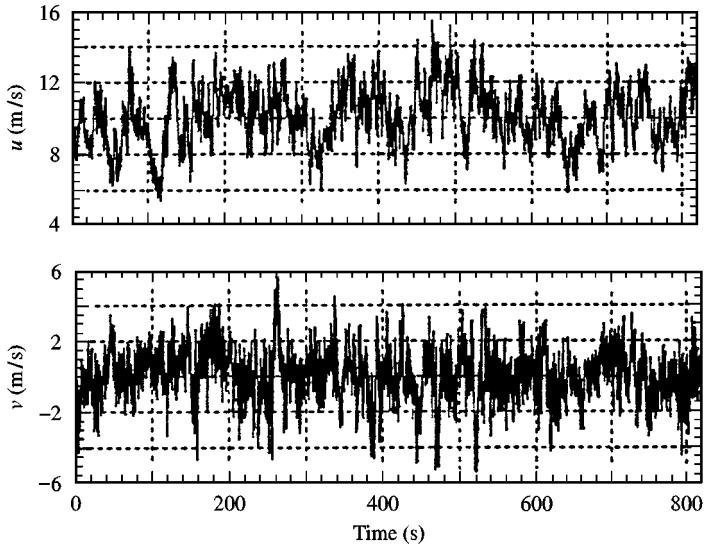

Figure 2. Time traces of the u- and v-velocity components.

densities of the u- and v-velocity records, shown in Figure 2, are presented in Figure 4. One feature that is displayed in these plots is the intermittency of each scale. The high contours represent "pulses" of energy of a certain scale over a certain time. For both velocity components, it is obvious that, for the large scales ($\ln a \geqq 3{\cdot}0, f_p < 0{\cdot}14$ Hz), the energy is not

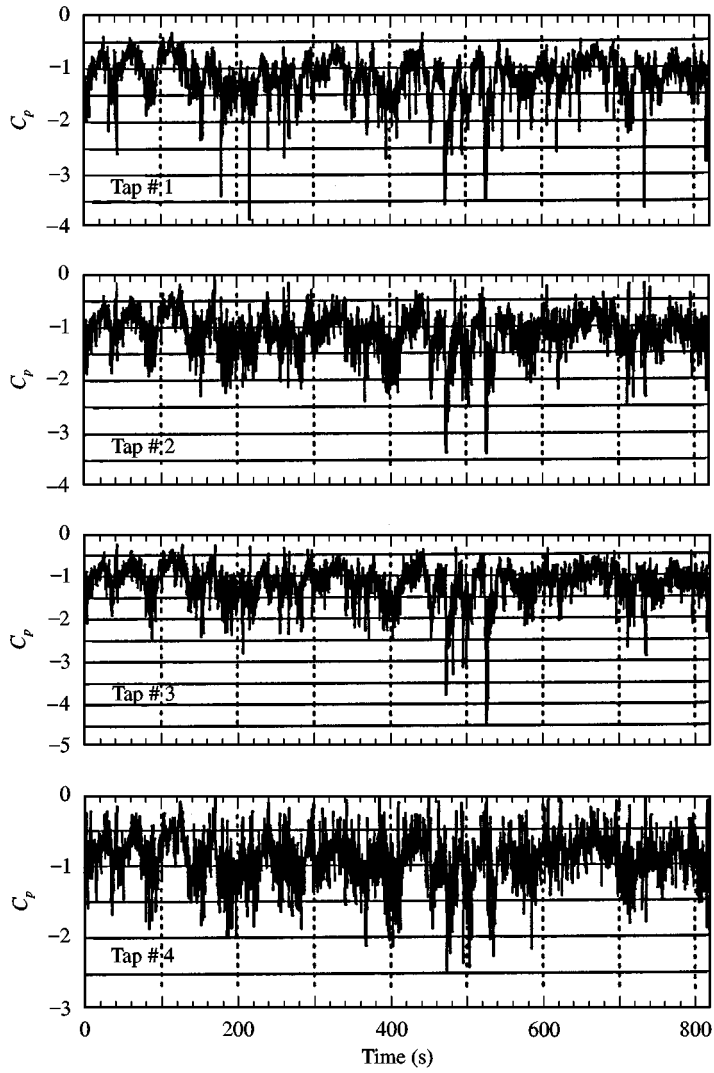

Figure 3. Time traces of the pressure coefficients at four different taps on the roof of the WERFL building.

evenly distributed in time. One can also note that these peaks are accompanied by intermittent streaks that extend over a scale range given by $\ln a$ between 1·5 and 3·9 ($0{\cdot}06 < f_p < 0{\cdot}65$ Hz). Corresponding contour plots of the wavelet energy density of the pressure coefficient, shown in Figure 3, are presented in Figure 5. These plots also show a high level of intermittency with relatively large values at locations where low pressure peaks are observed in the time series. These peaks extend over a scale range given by $\ln a$ between 2·0 and 4·0 ($0{\cdot}05 < f_p < 0{\cdot}4$ Hz).

Several important conclusions, regarding the velocity–pressure relation, can be drawn from the wavelet energy densities in Figure 4 and 5. First, the large-scale fluctuations of the u- and v-velocity components and the pressure are intermittent. As discussed in Section 2,

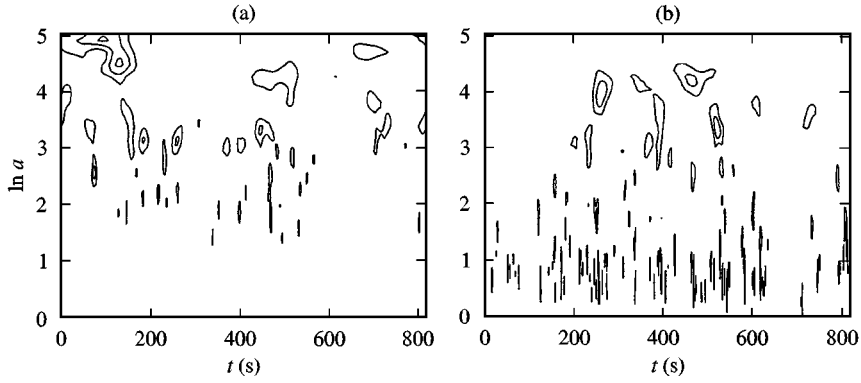

Figure 4. Contour plots of the wavelet energy density of the (a) u- and (b) v-velocity components shown in Figure 2.

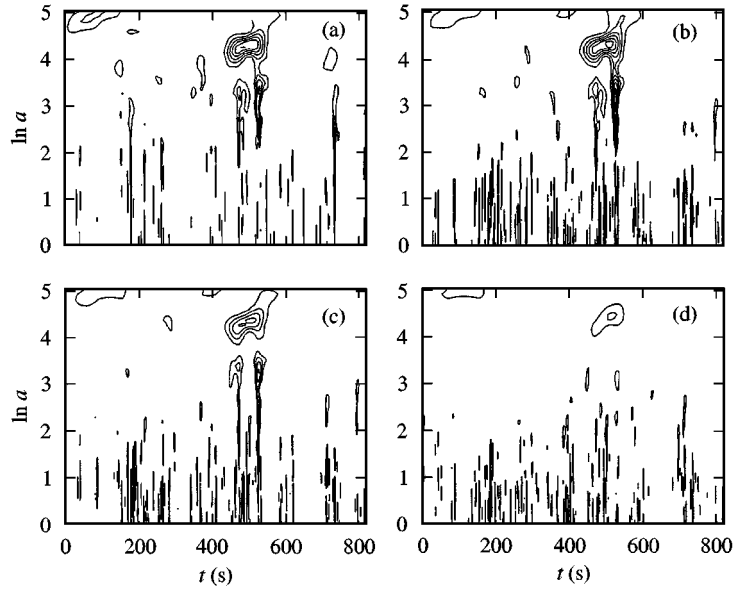

Figure 5. Contour plots of the wavelet energy density of the pressure coefficients at (a) tap #1, (b) tap #2, (c) tap #3, and (d) tap #4.

this high degree of intermittency is important to the usefulness of wavelet cross-scalogram results. Second, high values in the wavelet energy densities of pressure correspond to the low-pressure peaks. Third, the peak contour levels of the wavelet energy density representing the pressures at the four taps correspond to the level of the observed peaks of the time records. For instance, because the peaks of tap 4 have a lower value than those in taps 1, 2 and 3, the wavelet energy density at tap 4 has a lower magnitude than the wavelet energy densities at taps 1, 2 and 3.

In order to assess the velocity–pressure relation better, the wavelet cross- scalogram is used. The cross-scalogram gives peaks where fluctuations from two time series coincide in

scale and time. If fluctuations do not appear at the same time and same scale, the magnitude of the cross-scalogram is very low. By using the cross-scalogram between the velocity components and surface pressure fluctuations from several taps, one can examine the role of different turbulence scales in causing low-pressure peaks i.e. excessive wind loads, over an area. Figures 6 and 7 show that the $u - p$ and $v - p$ cross-scalograms for the records shown in figures 2 and 3. Both Figures 6 and 7 show that energetic events in velocity and pressure fluctuations take place at the same scale and time. The figures show that, for all taps, there is a coincidence between the scales with $\ln a$ near 4·0 ($f_p \simeq 0{\cdot}05$ Hz) of velocity and pressure fluctuations at times between 450 and 550 s. It is during these times that the pressure time series show large negative peaks. Note also that the contour peaks of tap 4 have lower values than those observed in taps 1, 2 and 3, which explains why the magnitude of the cross-scalogram is lower for that tap. It is important to note here that the peaks observed around $t = 100$ s are contaminated by end effects and thus do not give an accurate representation of the velocity–pressure relation near that time. The cross-scalogram results enable us to establish that there is a relation between time-localized fluctuations of u- and v-velcoity components and low-pressure peaks. Specifically, pressure fluctuations associated with peak negative pressures observed over a large area have the same scale as the velocity fluctuations in the same time interval. It must also be stressed that variations in the v-component of velocity are as important to the occurrence of low-pressure as variations in the u-component.

The results shown in this paper also illustrate an important feature of wavelet analysis: namely, that there is a finite temporal resolution that varies as a function of scale. As discussed by Farge (1992), the influence cone of wavelet coefficients that correspond to

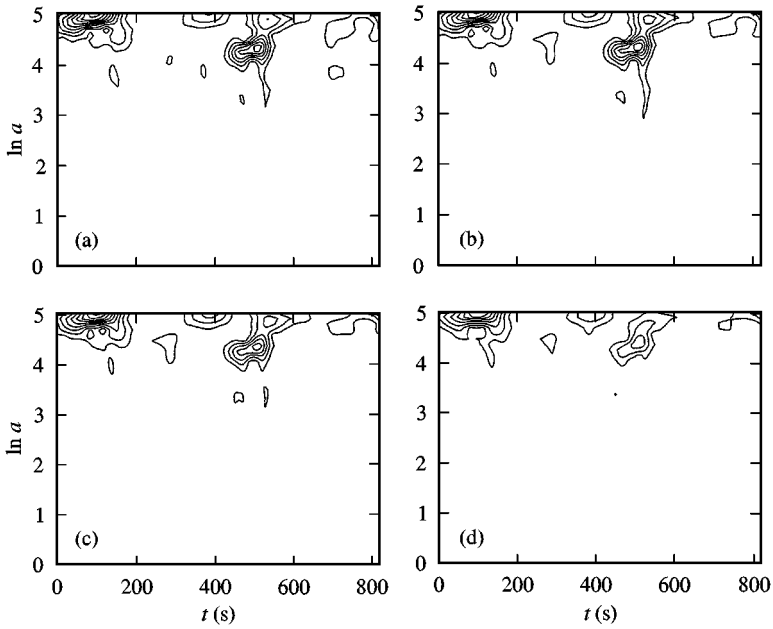

Figure 6. Contour plots of the cross-scalogram between the u-component and the pressure coefficients at (a) tap #1, (b) tap #2, (c) tap #3, and (d) tap #4.

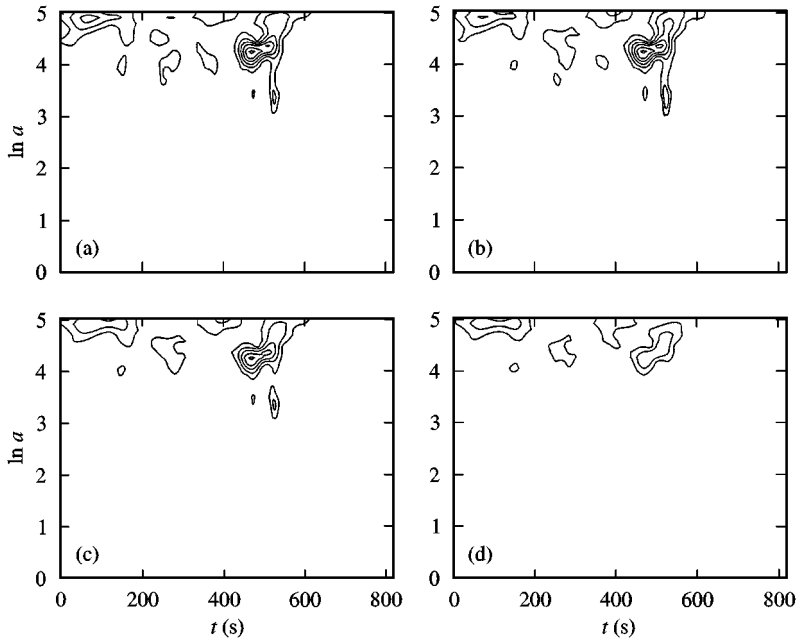

Figure 7. Contour plots of the cross-scalogram between the v-component and the pressure coefficients at (a) tap #1, (b) tap #2, (c) tap #3, and (d) tap #4.

a time in the fluctuation, t_0, for a mother wavelet that extends over $2T$ (where $T = 3\sigma_t$) is given by

$$t \in [t_0 - aT, t_0 + aT]. \tag{6}$$

Therefore, the influence of an event spreads in time as the scale increases. Note that the wavelet transform is linear, and superposition holds, ie

$$\mathscr{W}(a, \tau)[f] + \mathscr{W}(a, \tau)[g] = \mathscr{W}(a, \tau)[f + g], \tag{7}$$

where f and g are functions of time. However, the addition of complex quantities results in constructive and destructive interference of wavelet coefficients from two distinct events in a time series. The wavelet coefficients from two different times will begin to interfere at a scale where the influence cones of the two events begin to overlap. Therefore, some scales of the single event will be reinforced and others will be cancelled out. Clearly, the form of the interference pattern is dependent upon the scale content of the events and their separation distance.

In the pressure fluctuation plots, the two peak events are separated by 40 s. In this work, where the sampling rate of the time series is 10 Hz and the mother wavelet is sampled on 17 points, the influence cones of the peaks of the events begin to overlap at a scale $a = 40/1{\cdot}7 = 23{\cdot}52$ or $\ln a = 3{\cdot}15$. The other points of the event that are closer in time obviously begin to show interference at a smaller scale. When examining Figure 4, one observes what appears to be an interference pattern between the two peak events at 480 and 520 s. At scale values just above $\ln a = 4{\cdot}0$ ($f_p < 0{\cdot}05$ Hz), there are high contours stretching across the time interval between the two events. In fact, at this scale, the two events are

nearly indistinguishable. Just below $\ln a = (f_p > 0{\cdot}05\,\text{Hz})$, the values of the wavelet energy density decay only to increase again where the coefficients for each individual event are distinguishable and appear as streaks. This structure of the coefficients strongly suggests that there is an interference pattern between the two events.

The importance of this interference concept is that the scales associated with an event vary to some extent, depending on the content of the fluctuation within the influence cone of the event. In other words, the peaks in scale may appear to shift around from event to event. This illustrates the importance of analysing the peak events of many records to establish statistically what are the most significant scales in the flow that contribute to pressure peaks. That there is some variation in scale content from event to event does not lessen the significance of the cross-scalogram results. In fact, when viewing the cross-scalogram results it appears that the events in the velocity fluctuations exhibit a similar interference pattern.

4. CONCLUSIONS

In this work, the relation between velocity components of the atmospheric wind and pressure fluctuations at several taps on the roof of a low-rise building is examined in the time-scale domain. The continuous wavelet transform is applied to simultaneously measured velocity and pressure fluctuations. The wavelet energy densities show that the energy content of the large scales of the u- and v-velocity components is highly intermittent. The low-pressure peaks are represented in the time-scale domain by energetic events that are given by high levels of the wavelet energy density of the pressure fluctuations. In order to better assess the pressure–velocity relation, cross-scalogram analysis was performed on the simultaneously measured velocity and pressure fluctuations. The results show a relation between the time-localized events of u- and v-velocity components and the pressure peaks. More particularly, energetic events take place at the same time and at the same scale in both velocity and pressure fluctuations. Moreover, the results show that variations in the v-component of velocity are as important to the occurrence of peak pressures as variations in the u-component. Time-resolution considerations are also addressed, explaining that one might expect some variation in the scales associated with events in the time series depending on the type of fluctuations that appear near an event of interest.

The above results are of importance for the simulation and design of wind loads on structures. They establish the need for simulating events rather than merely matching integral length scales, mean flow parameters and/or turbulence intensity for the simulation of pressure peaks. Furthermore, the simulations should be able to reproduce characteristics described here, such as the large area effect of the turbulent events on the pressure field. By conducting further experiments and quantifying more results, one can establish a quantitative relation between events in the atmospheric boundary layer and pressure loading on structures. The results also illustrate the motivation and utility of continuing the improvement of understanding the finer points of wavelet analysis. These objectives are the subject of our ongoing research.

ACKNOWLEDGEMENTS

The financial support of the National Science Foundation under Grant # CMS-9412905 is greatly acknowledged. The authors wish to also thank Dr K. Mehta and his staff for providing the WERFL data and Mr Craig Lusk for his help in reproducing many of the plots.

References

FARGE, M. 1992 Wavelet transforms and their applications to turbulence. *Annual Review of Fluid Mechanics* **24,** 395–457.

HAJJ, M. R., JANAJREH, I. M., TIELEMAN, H. W. & REINHOLD, T. A. 1996 On frequency domain analysis of the relation between incident turbulence and fluctuating pressures. *Journal of Wind Engineering and Industrial Aerodynamics* **69-71,** 539–545.

HAJJ, M. R. & TIELEMAN, H. W. 1996 Application of wavelet analysis to incident wind in relevance to wind loads on structures. *ASME Journal of Fluids Engineering* **118,** 874–876.

HUDGINS, L., FRIEHE, C. A. & MAYER, M. E. 1993 Wavelet Transforms and Atmospheric Turbulence. *Physical Review Letters* **71,** 3279–3282.

JORDAN, D. A., HAJJ, M. R. & TIELEMAN, H. W. 1997 Characterization of turbulence scales in the atmospheric surface layer with the continuous wavelet transform. *Journal of Wind Engineering and Industrial Aerodynamics* **69-71,** 709–716.

JORDAN, D. A. MIKSAD, R. W. & POWERS, E. J. 1997 Implementation of the continuous wavelet transform for digital time series analysis. *Review of Scientific Instrumentation* **68,** 1484–1494.

KAWAI, H. 1983 Pressure fluctuations on square prisms: applicability of strip and quasi-steady theories. *Journal of Wind Engineering and Industrial Aerodynamics* **13,** 197–208.

KUMAR, P. & FOUFOULA-GEORGIOU, E. 1994 Wavelet analysis in geophysics: an introduction. In *Wavelet Analysis and its Applications*, *Vol. 4*: *Wavelets in Geophysics* (eds E. Foufoula- and Kumar), pp. 1–43. New York: Academic Press.

LEVITAN, M. L. & MEHTA, K. C. 1991 Texas Tech field experiments for wind loads; part I: building and pressure measurement system. *Journal of Wind Engineering and Industrial Aerodynamics* **41-44,** 1569–1576.